



Article

Enhanced Thermoelectric Performance of $\text{Na}_{0.55}\text{CoO}_2$ Ceramics Doped by Transition and Heavy Metal Oxides

Natalie S. Krasutskaya ¹, Andrei I. Klyndyuk ^{1,*}, Lyudmila E. Evseeva ², Nikolai N. Gundilovich ³, Ekaterina A. Chizhova ¹ and Andrei V. Paspelau ⁴

¹ Department of Physical, Colloid and Analytical Chemistry, Organic Substances Technology Faculty, Belarusian State Technological University, Sverdlova St. 13a, 220006 Minsk, Belarus; krasutskaya@belstu.by (N.S.K.); chizhova@belstu.by (E.A.C.)

² Thermophysical Measurement Lab, A.V. Luikov Heat and Mass Transfer Institute of the National Academy of Sciences of Belarus, Brovki St. 15, 220072 Minsk, Belarus; evseeva@itmo.by

³ Department of Glass and Ceramics Technology, Chemical Technology and Engineering Faculty, Belarusian State Technological University, Sverdlova St. 13a, 220006 Minsk, Belarus; gundilovich@belstu.by

⁴ Physical and Chemical Investigations Methods Center, Belarusian State Technological University, Sverdlova St. 13a, 220006 Minsk, Belarus; andrei29088@mail.ru

* Correspondence: klyndyuk@belstu.by; Tel.: +375-(29)-636-5624

Abstract: Using the solid-state reactions method $\text{Na}_{0.55}(\text{Co},\text{M})\text{O}_2$ ($\text{M} = \text{Cr}, \text{Ni}, \text{Zn}, \text{W}$, and Bi) ceramics were prepared and their crystal structure, microstructure, electrophysical, thermophysical, and thermoelectric properties were studied. Doping of $\text{Na}_{0.55}\text{CoO}_2$ by transition or heavy metal oxides led to the increase in the grain size of ceramics, a decrease in electrical resistivity and thermal diffusivity values, and a sharp increase in the Seebeck coefficient, which resulted in essential enhancement of their thermoelectric properties. The largest power factor ($1.04 \text{ mW}/(\text{m}\cdot\text{K}^2)$ at 1073 K) and figure of merit (0.702 at 1073 K) among the studied samples possessed the $\text{Na}_{0.55}\text{Co}_{0.9}\text{Bi}_{0.1}\text{O}_2$ compound, which also demonstrated the highest values of the Seebeck coefficient ($666 \mu\text{V}/\text{K}$ at 1073 K). The obtained results show that the doping of layered sodium cobaltite by different metal oxides allows for improving its stability, microstructure, and functional properties, which proves the effectiveness of the doping strategy for developing new thermoelectric oxides with enhanced thermoelectric performance.



Citation: Krasutskaya, N.S.; Klyndyuk, A.I.; Evseeva, L.E.; Gundilovich, N.N.; Chizhova, E.A.; Paspelau, A.V. Enhanced Thermoelectric Performance of $\text{Na}_{0.55}\text{CoO}_2$ Ceramics Doped by Transition and Heavy Metal Oxides. *Solids* **2024**, *5*, 267–277. <https://doi.org/10.3390/solids5020017>

Academic Editor: Andrei Kovalevsky

Received: 15 March 2024

Revised: 12 April 2024

Accepted: 25 April 2024

Published: 3 May 2024



Copyright: © 2024 by the authors. Licensee MDPI, Basel, Switzerland. This article is an open access article distributed under the terms and conditions of the Creative Commons Attribution (CC BY) license (<https://creativecommons.org/licenses/by/4.0/>).

1. Introduction

Waste heat, evolving into the environment by industrial enterprises, cars, and households, can be directly and effectively converted into electrical energy using thermoelectric generators (TEGs). The concept of TEGs can be realized with the use of thermoelectric materials, which should possess at the same time both low thermal conductivity (λ) and electrical resistivity (ρ) and high values of the Seebeck coefficient (S) [1–5]. Due to the strong interconnection of the above mentioned properties, the number of thermoelectric materials is strongly restricted. Nevertheless, since the 1960s, a number of effective thermoelectrics have been developed, which are successfully used in the production of thermoelectric devices of different purposes (TEGs, thermoelectric refrigerators (coolers), thermocouples, etc.) [6–8]. Traditional thermoelectrics on the base of layered chalcogenides of bismuth and tellurium possess several drawbacks since they contain toxic, rare, and expensive components, are unstable in the air at high temperatures due to oxidation by atmospheric oxygen, etc. Nevertheless, such drawbacks are absent for oxide thermoelectrics [9–13]. One of the well-known representatives of thermoelectrics is layered sodium cobaltite first characterized by Terasaki et al. [14]. Having unique electrotransport properties, layered sodium cobaltite is tested as a possible material for p -branches of TEGs [6,7,15], cathode material for sodium-ion batteries (SIBs), etc. [16–19]. Its crystal hydrate, $\text{Na}_x\text{CoO}_2 \cdot y\text{H}_2\text{O}$,

below 4 K undergoes a transition into a superconducting state [20]. The physicochemical and functional properties of Na_xCoO_2 strongly depend on the sodium content (x_{Na}) [21,22], which also determines the phase structure.

Sodium cobaltite, $\alpha\text{-Na}_x\text{CoO}_2$ ($0.9 \leq x \leq 1.0$) possesses an $O3$ structure, $\alpha'\text{-Na}_x\text{CoO}_2$ has an $O'3$ structure (monoclinically distorted $O3$ phase), $\beta\text{-Na}_x\text{CoO}_2$ ($0.55 \leq x \leq 0.6$) has a $P3$ structure, and $\gamma\text{-Na}_x\text{CoO}_2$ ($0.55 \leq x/y \leq 0.74$) has a $P2$ -structure [23]. The letter characterizes the oxygen setting of sodium (octahedral (O) or prismatic (P)), and the number (two or three) shows the quantity of CoO_2 layers in the c period of the Na_xCoO_2 crystal lattice.

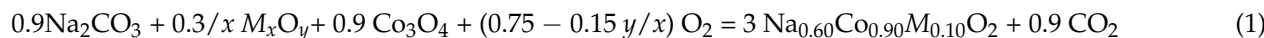
Different approaches are used to improve the thermoelectric and other functional properties of Na_xCoO_2 : (i) doping strategy (in sublattices of sodium [24,25] or cobalt [26–29]), (ii) modification strategy (by metals [30,31], reduced graphene oxide [32], etc.), and (iii) microstructure regulation strategy [33–35], etc.

In our previous works [36,37], we estimated the possibility of improving the thermoelectric performance of Na_xCoO_2 by its doping for different transition and non-transition metal oxides.

The aim of this study was to examine the effect of Na_xCoO_2 doping by some transition (Cr_2O_3 , NiO and ZnO) and heavy metal oxide (WO_3 and Bi_2O_3) on the crystal structure, microstructure, stability, electron transport, and thermophysical and thermoelectric properties of the obtained $\text{Na}_x\text{Co}_{0.90}M_{0.10}\text{O}_2$ ($M = \text{Cr}, \text{Ni}, \text{Zn}, \text{W}$ and Bi) complex oxides.

2. Materials and Methods

Ceramic samples of $\text{Na}_{0.60}\text{Co}_{0.90}M_{0.10}\text{O}_2$ ($M = \text{Cr}, \text{Ni}, \text{Zn}, \text{W}$, and Bi) materials were prepared by the solid-state reactions method following the reaction scheme:



Powders of Na_2CO_3 (99%), Co_3O_4 (99%), Cr_2O_3 (99%), NiO (99.99%), WO_3 (99.99%), and Bi_2O_3 (99.99%) were mixed in proportions of $\text{Na}: \text{Co}: M = 0.6: 0.9: 0.1$. The excess amount of Na_2CO_3 was introduced in the batch to compensate for the losses of the Na_2O in the ceramics due to its high-temperature treatment and to obtain the samples of the following composition $\text{Na}_{0.55}(\text{Co}, M)\text{O}_2$ ($M = \text{Cr}, \text{Ni}, \text{Zn}, \text{W}$, and Bi) [21,38]. Weighed batches were mixed with $\text{C}_2\text{H}_5\text{OH}$ (~3–5 wt.%) and then milled in a PM 100 Retsch planetary mill (material of beakers and grinding balls is ZrO_2) for 90 min at 300 rpm. Obtained slurries were dried and pressed in the form of tablets with a diameter of 19 mm and height of 2–3 mm. Afterward, the as-obtained samples were calcined in air for 12 h at a temperature of 1133 K. After calcination, the samples were crushed in an agate mortar, then milled in the planetary mill and pressed in the form of bars with dimensions of $5 \times 5 \times 30 \text{ mm}^3$ and tablets having a diameter of 15 mm and height of 2–3 mm, which were sintered in air for 12 h at a temperature of 1203 K [36].

According to [39,40], the oxygen sublattice of Na_xCoO_2 layered cobaltite contains a negligible quantity of vacancies, so the oxidation degree of cobalt in these phases is controlled only by the content of sodium (x_{Na}) in them ($\text{Na}_x^{+1}\text{Co}_{1-x}^{+4}\text{Co}_x^{+3}\text{O}_2$). The average oxidation degree of cobalt and real sodium content in the obtained ceramic materials were determined by means of iodometric [38] and reverse potentiometric titration [41] (see Supplementary Information).

The phase identification of the samples and calculation of their lattice parameters were performed by means of X-ray diffraction analysis (XRD) using Bruker D8 XRDAvance X-ray diffractometer $\text{CuK}\alpha$ radiation ($\lambda = 1.5406 \text{\AA}$). The values of the coherent scattering area for the $\text{Na}_{0.55}\text{Co}_{0.90}M_{0.10}\text{O}_2$ ceramics were calculated using the Debye–Sherrer equation (D_S) (2) [42] and the size-strain (D_{SS}) method (3) [43]:

$$D_S = (0.9\lambda)/(\beta \times \cos\Theta), \quad (2)$$

$$(d \times \beta \times \cos\Theta) = (0.9\lambda/D_{SS})(d^2 \times \beta \times \cos\Theta) + (\varepsilon/2)^2 \quad (3)$$

where d is the interplanar distance, nm, β is the full width of the reflex at its half maxima, rad, Θ is the diffraction angle, ° and ε is the microstrain.

The degree of crystallographic orientation of the grains of $\text{Na}_{0.55}\text{Co}_{0.90}\text{M}_{0.10}\text{O}_2$ ceramics was estimated via the Lotgering factor [3,44]:

$$f = (p - p_0)/(1 - p_0) \quad (4)$$

where $p = \Sigma I(00l)/\Sigma I(hkl)$ (ΣI is the sum of the counts of X-ray diffraction peaks of the synthesized samples) and $p_0 = \Sigma I_0(00l)/\Sigma I_0(hkl)$ (ΣI_0 is the sum of the counts of X-ray diffraction peaks of the randomly oriented sample). Here p_0 was calculated from the peak intensities of the reference phase (JCPDC #00-030-1182)).

The apparent density of synthesized ceramics (d_{EXP}) was determined from the mass and geometrical dimensions of the samples, and their total porosity (Π_t) was calculated as

$$\Pi_t = (1 - d_{\text{EXP}}/d_{\text{XRD}}) \times 100\%. \quad (5)$$

where d_{XRD} is the X-ray density of the samples in g/cm^3 .

The open porosity of the samples (Π_o) was determined by weighing the samples of $\text{Na}_{0.55}\text{Co}_{0.90}\text{M}_{0.10}\text{O}_2$ ceramics saturated by ethylacetate for 45 min under a vacuum of 25–30 Pa and introduced into the liquid ethylacetate following the equation:

$$\Pi_o = ((m_1 - m)/(m_1 - m_2)) \times 100\% \quad (6)$$

where m is the mass of the dry ceramic sample g; m_1 and m_2 are the masses of the sample saturated by the liquid ethylacetate at weighing in the air and introduced into the liquid ethylacetate, respectively.

The microstructure and chemical composition of the $\text{Na}_{0.55}\text{Co}_{0.90}\text{M}_{0.10}\text{O}_2$ samples were studied using scanning electron microscopy (SEM) by a JEOL JSM-5610LV scanning electron microscope equipped with an EDX JED-2201 X-ray energy dispersive chemical analysis system.

The electrical resistivity (ρ) and the Seebeck coefficient (S) of the sintered ceramics were measured in the air within a temperature interval of 323–1073 K following the procedure described in [36].

The thermal diffusivity (η) of the layered cobaltites was studied in the helium atmosphere within the temperature interval of 323–1073 K by means of an LFA 457 MicroFlash device (NETZSCH). The thermal conductivity of $\text{Na}_{0.55}\text{Co}_{0.90}\text{M}_{0.10}\text{O}_2$ sintered ceramics was calculated by the equation

$$\lambda = \eta \times d_{\text{EXP}} \times Cp \quad (7)$$

where Cp is heat capacity, calculated by the Dulong–Petit law. This approach can be used for the estimation of the Cp values of ceramics examined. As in [45], it was found that the heat capacity of the layered sodium cobaltite near 300 K becomes slightly dependent on temperature and reaches a plateau.

The phonon (λ_{ph}) and electronic (λ_{el}) parts of the thermal conductivity of ceramics were roughly approximated by Equations (8) and (9)

$$\lambda = \lambda_{\text{el}} + \lambda_{\text{ph}} \quad (8)$$

$$\lambda_{\text{el}} = (L \times T)/\rho \quad (9)$$

where L is Lorentz number ($L = 2.45 \times 10^{-8} \text{ W} \times \Omega \times \text{K}^{-2}$).

The values of power factor (P) and figure of merit (ZT) of the $\text{Na}_{0.55}\text{Co}_{0.90}\text{M}_{0.10}\text{O}_2$ layered oxides were calculated as

$$P = S^2 / \rho \quad (10)$$

and

$$ZT = (P \times T)/\lambda. \quad (11)$$

3. Results and Discussion

The sodium content in the as-obtained samples (x_{Na}), determined by iodometry and reverse potentiometry, was about 0.55 for all the samples under study (Table 1). The average oxidation state of cobalt in $\text{Na}_{0.55}\text{Co}_{0.90}M_{0.10}\text{O}_2$ ($M = \text{Cr}, \text{Co}, \text{Ni}, \text{Zn}, \text{W}$, and Bi) layered cobaltites varied within 3.17–3.61 (Table 1), increasing in the case of the substitution of the acceptor character (Ni or Zn instead of Co) and decreasing at the substitution of the donor character (W or Bi instead of Co).

Table 1. Values of sodium content (x_{Na}), the oxidation state of cobalt (Co^{+z}), lattice constants (a, c , $c/a, V$), Lotgering factor (f), size of the coherent scattering area obtained using the Scherrer equation (D_s), and the size-strain method (D_{SS}), microstrain (ε), and X-ray density (d_{XRD}) of ceramic samples $\text{Na}_{0.55}\text{Co}_{0.90}M_{0.10}\text{O}_2$ ($M = \text{Cr}, \text{Ni}, \text{Zn}, \text{W}$, and Bi).

M	x_{Na}	z	$a, \text{\AA}$	$c, \text{\AA}$	c/a	$V, \text{\AA}^3$	f	D_s, nm	D_{SS}, nm	$\varepsilon \times 10^4$	$d_{\text{XRD}}, \text{g/cm}^3$
Cr	0.552	3.50	2.840	10.91	3.841	76.21	0.82	73	61	3.285	4.48
Co	0.545	3.45	2.824	10.99	3.892	75.87	0.35	48	46	3.521	4.54
Ni	0.559	3.61	2.824	10.95	3.879	75.66	0.60	62	53	1.257	4.55
Zn	0.548	3.61	2.849	10.91	3.830	76.70	0.64	71	61	0.680	4.51
W	0.551	3.17	2.837	10.89	3.839	75.91	0.89	78	64	3.448	5.08
Bi	0.553	3.28	2.839	10.61	3.842	76.13	0.87	65	56	2.833	5.17

The obtained samples of $\text{Na}_{0.55}\text{Co}_{0.90}M_{0.10}\text{O}_2$ ($M = \text{Cr}, \text{Ni}, \text{Zn}, \text{W}$, and Bi), like $\text{Na}_{0.55}\text{CoO}_2$ base cobaltite, possessed a hexagonal structure, which corresponds to the structure of $\gamma\text{-Na}_x\text{CoO}_2$ phase [46,47] (Figure 1a). Additionally, the reflexes of the impurity phase, Co_3O_4 , were identified in their powder diffractograms.

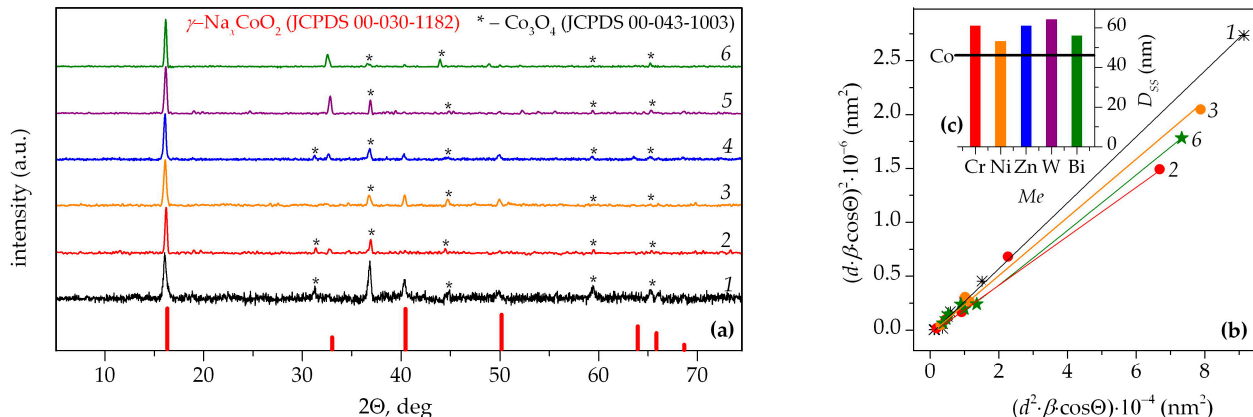


Figure 1. X-ray powder diffractograms ($\text{CuK}\alpha$ -radiation) (a), size-strain plots (b), and coherent scattering area (c) for $\text{Na}_{0.55}\text{CoO}_2$ (1) sodium cobaltite and $\text{Na}_{0.55}\text{Co}_{0.90}M_{0.10}\text{O}_2$ ($M = \text{Cr}$ (2), Ni (3), Zn (4), W (5), and Bi (6)) solid solutions.

This phase forms due to the partial degradation of the ceramic surface by its interaction with the CO_2 and H_2O vapors present in an atmosphere according to the reactions (12) and (13):



The reflex intensities of the Co_3O_4 phase for $\text{Na}_{0.55}\text{Co}_{0.90}M_{0.10}\text{O}_2$ compounds were essentially smaller than those for the base $\text{Na}_{0.55}\text{CoO}_2$ phase (Figure 1a), and the content of Co_3O_4 oxide in these materials estimated using methods described in [48], was equal to 30 mol.% for $\text{Na}_{0.55}\text{CoO}_2$, 16 mol.% for $M = \text{W}$, 15 mol.% for $M = \text{Cr}$, and Ni , 12 mol.% for $M = \text{Zn}$, and 8 mol.% for $M = \text{Bi}$. The obtained results indicated the increase in the

chemical stability of the layered sodium cobaltite in an atmosphere of wet air at its doping by transition or heavy metal oxides due to the increase of the metal–oxygen interactions in their structure.

The values of the a lattice constant of the $\text{Na}_{0.55}\text{Co}_{0.90}\text{M}_{0.10}\text{O}_2$ solid solution slightly increased, but the c lattice constant decreased compared to the parent phase of $\text{Na}_{0.55}\text{CoO}_2$ (Table 1). As a result, the values of volume of the unit cell of $\text{Na}_{0.55}\text{Co}_{0.90}\text{M}_{0.10}\text{O}_2$ cobaltites at the variation of their cationic composition retained almost unchanged, but their axial ratio essentially decreased at the partial substitution of cobalt by other metals in $\text{Na}_{0.55}\text{CoO}_2$. Such a substitution slightly affects the size of the unit cell of layered sodium cobaltite but results in its significant deformation—contraction in the direction of the c axis (perpendicular to the conducting $-\text{[CoO}_2-$ layers) and enlarging in the direction of the a axis (parallel to the conducting $-\text{[CoO}_2-$ layers).

The coherent scattering area of the $\text{Na}_{0.55}\text{Co}_{0.90}\text{M}_{0.10}\text{O}_2$ materials obtained using different approaches (Figure 1b) is essentially large (up to 29–63% and 15–35% according to the results of the Sherrer and size-strain methods, respectively) (Figure 1c, Table 1) than for the base-layered sodium cobaltite phase. In turn, the microstrain values of the $\text{Na}_{0.55}\text{Co}_{0.90}\text{M}_{0.10}\text{O}_2$ ceramics were slightly ($M = \text{Cr}$ and W) or essentially ($M = \text{Ni}$, Zn , and Bi) smaller in comparison to the parent $\text{Na}_{0.55}\text{CoO}_2$ cobaltite (Table 1).

The Lotgering factor values of the ceramics increased from 0.35 for $\text{Na}_{0.55}\text{CoO}_2$ (moderate orientation [44]) to 0.60–0.64 for $\text{Na}_{0.55}\text{Co}_{0.90}\text{M}_{0.10}\text{O}_2$ ($M = \text{Ni}$ and Zn) (good orientation [44]) and 0.82–0.89 for $\text{Na}_{0.55}\text{Co}_{0.90}\text{M}_{0.10}\text{O}_2$ ($M = \text{Cr}$, W , and Bi) (very good orientation [44]) (Table 1). Therefore, the doping of $\text{Na}_{0.55}\text{CoO}_2$ by different metal oxides increased the grain crystallographic orientation degree of the ceramics (its texturing degree). The most prominent effect among samples synthesized in this work was observed for $\text{Na}_{0.55}\text{Co}_{0.90}\text{W}_{0.10}\text{O}_2$.

The apparent density values of the $\text{Na}_{0.55}\text{Co}_{0.90}\text{M}_{0.10}\text{O}_2$ ceramics varied within 3.43–3.72 g/cm³ and decreased at the partial substitution of Co by Cr, Ni, or Zn and increased at the substitution of Co by W and Bi (Table 2). The open porosity values of ceramics varied within 17–22% and were close to each other for the samples having different cationic compositions. The closed porosity of the ceramics was negligible (Table 2).

Table 2. Values of apparent density (d_{EXP}), total (Π_t) and open (Π_o) porosity, electrical resistivity (ρ_{1073}), Seebeck coefficient (S_{1073}), power factor (P_{1073}), and figure of merit (ZT_{1073}) of $\text{Na}_{0.55}\text{Co}_{0.90}\text{M}_{0.10}\text{O}_2$ ($M = \text{Cr}$, Ni , Zn , W , and Bi) ceramics.

M	d_{EXP} , g/cm ³	Π_t , %	Π_o , %	$10^4 \times \rho_{1073}, \Omega \times \text{m}$	S_{1073} , $\mu\text{V/K}$	P_{1073} , $\text{mW}/(\text{m} \times \text{K}^2)$	ZT_{1073}
Cr	3.48	17	22	3.44	540	0.846	0.565
Co	3.65	18	18	4.82	285	0.169	0.233
Ni	3.43	22	23	5.13	608	0.721	0.622
Zn	3.59	21	17	3.03	421	0.584	0.523
W	3.92	17	17	5.20	620	0.740	0.643
Bi	3.72	21	17	4.28	666	1.038	0.702

According to the SEM results, the grains of the $\text{Na}_{0.55}\text{CoO}_2$ ceramics were plate-like, with dimensions (l) of 5–10 μm and thicknesses of 2–4 μm (average dimension (l_{av}) of about 8 μm and aspect ratio (AR) of about 2.7). The microstructure of the $\text{Na}_{0.55}\text{Co}_{0.90}\text{M}_{0.10}\text{O}_2$ materials was similar to the $\text{Na}_{0.55}\text{CoO}_2$ one but they differed in the size and aspect ratio (form) of the grains (Figure 2b–f). The grain size of the $\text{Na}_{0.55}\text{Co}_{0.90}\text{M}_{0.10}\text{O}_2$ ($M = \text{Cr}$, Ni , and Zn) ceramics was varied, within 8–15 μm with a thickness of 3–6 μm (l_{av} (AR) was about 11 μm (2.8), 13 μm (2.6), and 9 μm (1.8) for $M = \text{Cr}$, Ni , and Zn , respectively). Doping of layered sodium cobaltite ceramics with bismuth or tungsten oxides results in an increase of its grain size by up to 12–21 μm and a decrease of the thickness of the grains by up to 1–3 μm . For $\text{Na}_{0.55}\text{Co}_{0.90}\text{W}_{0.10}\text{O}_2$ and $\text{Na}_{0.55}\text{Co}_{0.90}\text{Bi}_{0.10}\text{O}_2$, the l_{av} (AR) values were equal to about 13 μm (7.5) and 16 μm (8.0), respectively. As a result, the anisotropy of grains of

layered sodium cobaltite ceramics increased at its doping by heavy metal oxides containing highly charged metal ions (Bi^{5+} , W^{6+}).

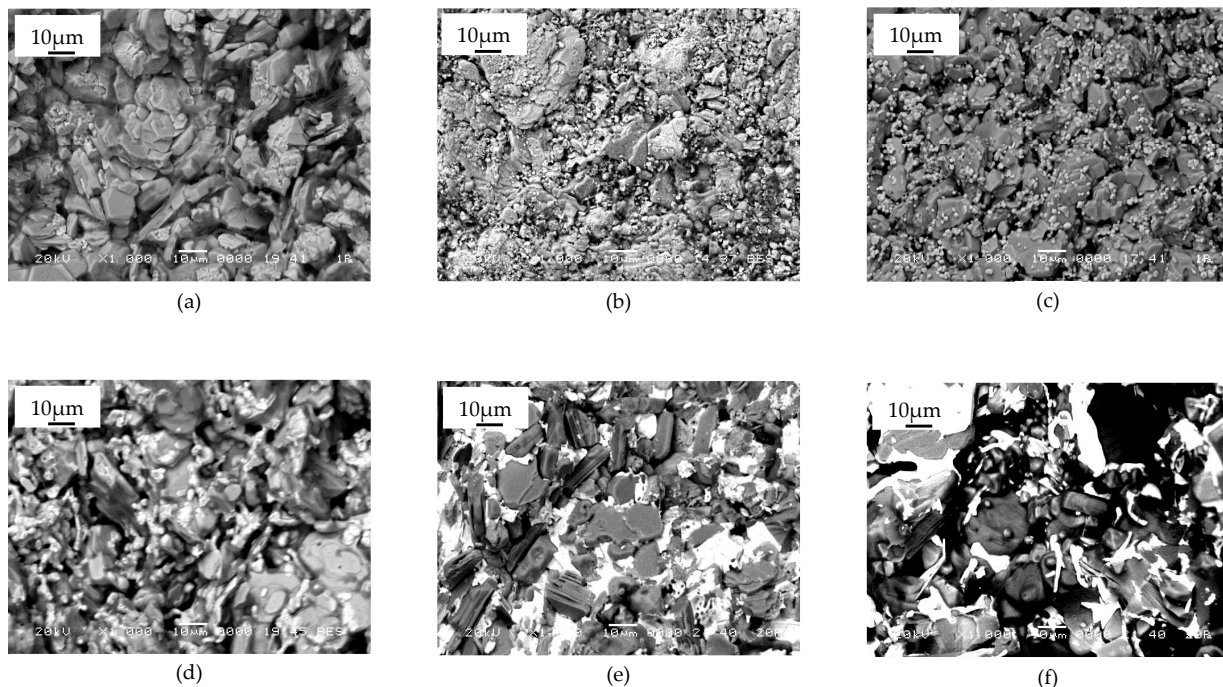


Figure 2. Electron micrographs of ceramic cleavages $\text{Na}_{0.55}\text{Co}_{0.90}\text{M}_{0.10}\text{O}_2$: $\text{M} = \text{Cr}$ (a), Co (b), Ni (c), Zn (d), W (e), and Bi (f)).

According to the EDX results (see Supplementary Information, Table S1) the cationic composition of the cobalt sublattice of the $\text{Na}_{0.55}\text{Co}_{0.90}\text{M}_{0.10}\text{O}_2$ compounds was close to the aim one, and the distribution of elements within the volume of ceramics was close to uniform (Figure 3).

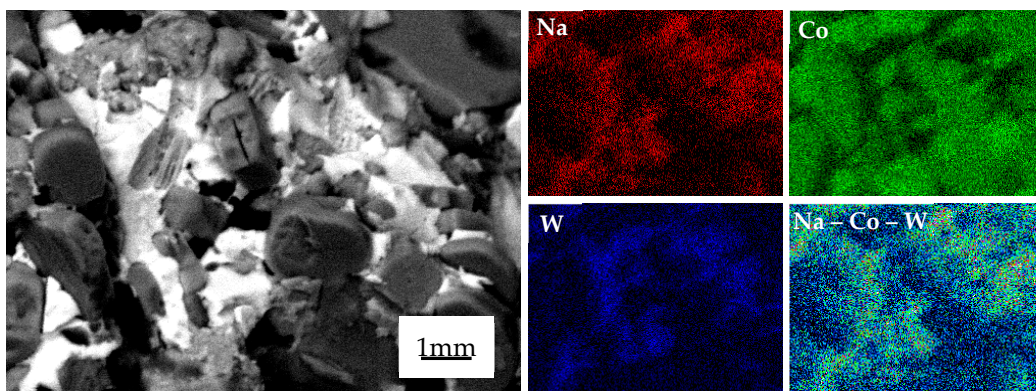


Figure 3. Element mapping images of the $\text{Na}_{0.55}\text{Co}_{0.90}\text{W}_{0.10}\text{O}_2$ ceramic sample.

As can be seen from Figure 4a, $\text{Na}_{0.55}\text{CoO}_2$ ceramics possess a metallic conductivity character ($\partial\rho/\partial T > 0$), which changed into a semiconducting one ($\partial\rho/\partial T < 0$) near 520 K, like the conductivity crossover in layered calcium cobaltite of $\text{Ca}_3\text{Co}_4\text{O}_{9+\delta}$ [49]. The electrical resistivity values of the Ni-doped sample are close to the $\text{Na}_{0.55}\text{CoO}_2$ ones, but $\text{Na}_{0.55}\text{Co}_{0.90}\text{Ni}_{0.10}\text{O}_2$ demonstrates only the semiconducting conductivity character within the whole studied temperature range. The other $\text{Na}_{0.55}\text{CoO}_2$ substitutes, like the parent phase, demonstrated conductivity crossover, but their temperature shifts to the higher values (for example, to ~720 K for $\text{Na}_{0.55}\text{Co}_{0.90}\text{Cr}_{0.10}\text{O}_2$ or ~920 K for $\text{Na}_{0.55}\text{Co}_{0.90}\text{W}_{0.10}\text{O}_2$ (Figure 4a)). The doping of layered sodium cobaltite by different metal oxides results in a

decrease its electrical resistivity values (Figure 4a,d, Table 2) due to the donor character of doping (W or Bi for Co), decreasing the grain boundaries density (increase of grains size), which serve as charge carriers scattering regions, and also due to the decreasing of high-resistive Co_3O_4 phase content in the samples [50] (Figure 1a). Note that the electrical resistivity values of all samples are getting closer at a high temperature. Therefore, ρ values of $\text{Na}_{0.55}\text{Co}_{0.90}M_{0.10}\text{O}_2$ ($M = \text{Ni}$ and W) at 1073 K are slightly larger, and for $\text{Na}_{0.55}\text{Co}_{0.90}M_{0.10}\text{O}_2$ ($M = \text{Cr}$, Zn , and Bi), they are comparatively smaller than those of $\text{Na}_{0.55}\text{CoO}_2$ (Figure 4d and Table 2).

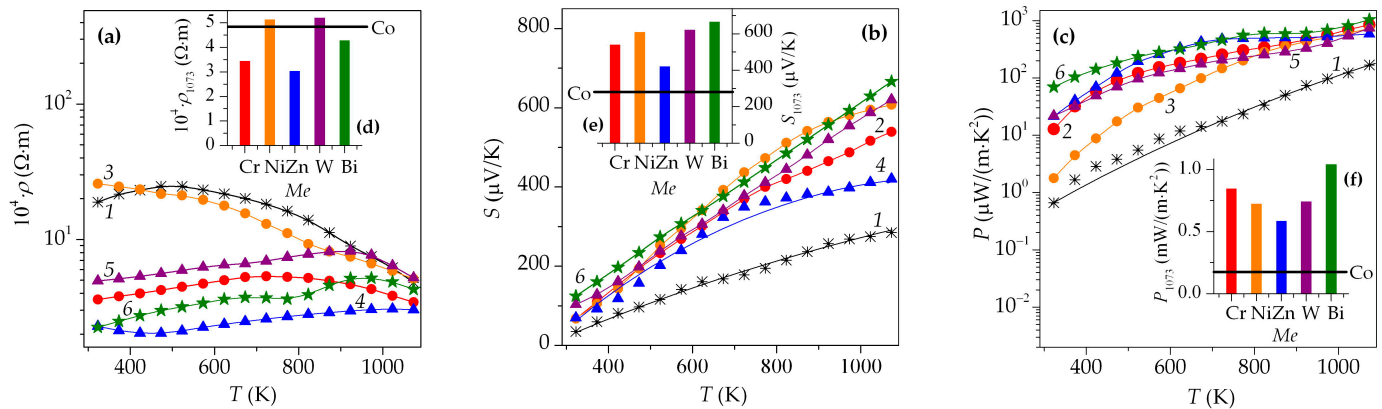


Figure 4. Temperature dependences of electrical resistivity ρ (a), Seebeck's coefficient S (b), and power factor P (c) of ceramic samples of $\text{Na}_{0.55}\text{CoO}_2$ sodium cobaltite (1) and $\text{Na}_{0.55}\text{Co}_{0.90}M_{0.10}\text{O}_2$ ($M = \text{Cr}$ (2), Ni (3), Zn (4), W (5), and Bi (6)) solid solutions. Insets show the electrical resistivity ρ_{1073} (d), Seebeck's coefficient S_{1073} (e), and power factor P_{1073} (f) values of $\text{Na}_{0.55}\text{Co}_{0.90}M_{0.10}\text{O}_2$ solid solutions compared to the $\text{Na}_{0.55}\text{CoO}_2$ phase.

The positive sign of the Seebeck coefficient (Figure 4b) of all the studied samples points out that holes are the main charge carriers, and they are *p*-type conductors. The change in the values of the Seebeck coefficient at high temperatures is practically linear (Figure 4b). This dependence follows Equation (14), usually used for the description of the thermoelectric properties of metals and degenerated semiconductors [3,4]:

$$S = [(8\pi^2 k_B^2)/(3eh)] \times m^* \times T \times (\pi/3n)^2/3 \quad (14)$$

where k_B is the Boltzmann constant, m^* is the density of a state's effective mass, h is the Planks constant, e is the charge of the electron, T is the absolute temperature, and n is the charge carrier's concentration.

Doping of $\text{Na}_{0.55}\text{CoO}_2$ by different transition or heavy metal oxides results in the sharp increase of its Seebeck coefficient, which is more pronounced at high temperatures (Figure 4b,e and Table 2). This is probably caused by an increase in the configurational entropy that is provided by the presence of Co in different charge (Co^{2+} , Co^{3+} , and Co^{4+}) and spin (high-, intermediate- and low-spin states) states [51]. The highest S values among the studied samples demonstrated that $\text{Na}_{0.55}\text{Co}_{0.90}\text{W}_{0.10}\text{O}_2$ and $\text{Na}_{0.55}\text{Co}_{0.90}\text{Bi}_{0.10}\text{O}_2$ complex oxides (620 and 666 $\mu\text{V}/\text{K}$ at 1073 K, respectively) are 2.18 and 2.33 times larger than for the parent $\text{Na}_{0.55}\text{CoO}_2$ phase (Figure 4e and Table 2). These phases are prospective materials for *p*-legs of ceramic (oxide) thermocouples. It should be noted that similar results were obtained when studying the Seebeck coefficient of cobalt-substituted derivatives of $\text{Ca}_3\text{Co}_4\text{O}_{9+\delta}$ layered cobaltite [52].

Power factor values of $\text{Na}_{0.55}\text{CoO}_2$ derivatives are essentially larger compared to the parent phase due to their low electrical resistivity and high Seebeck coefficient (Figure 4c,f and Table 2). They increased as the temperature increased and reached the maximum value of 0.846 and 1.038 $\text{mV}/(\text{m} \cdot \text{K}^2)$ for $\text{Na}_{0.55}\text{Co}_{0.90}\text{Cr}_{0.10}\text{O}_2$ and $\text{Na}_{0.55}\text{Co}_{0.90}\text{Bi}_{0.10}\text{O}_2$ ceramics,

respectively. That is 5.01 and 6.14 times larger than for the undoped sodium cobaltite (Table 2 and Figure 4e).

Both the thermal diffusivity and thermal conductivity values of $\text{Na}_{0.55}\text{Co}_{0.10}\text{M}_{0.10}\text{O}_2$ ceramics decreased as the temperature increased (Figure 5a,b) and increased at the doping of $\text{Na}_{0.55}\text{CoO}_2$ by different metal oxides (Figure 5d,e), probably mainly due to the increase of the ceramics' grains size, resulting in a decrease of the density of the grain boundaries, serving as effective regions of phonons scattering [37]. The electronic part of the thermal conductivity of the ceramics was relatively small ($\lambda_{\text{el}}/\lambda = 0.04\text{--}0.07$) and increased with temperature increase. The phonon part dominated and decreased at temperature gain (Figure 5c).

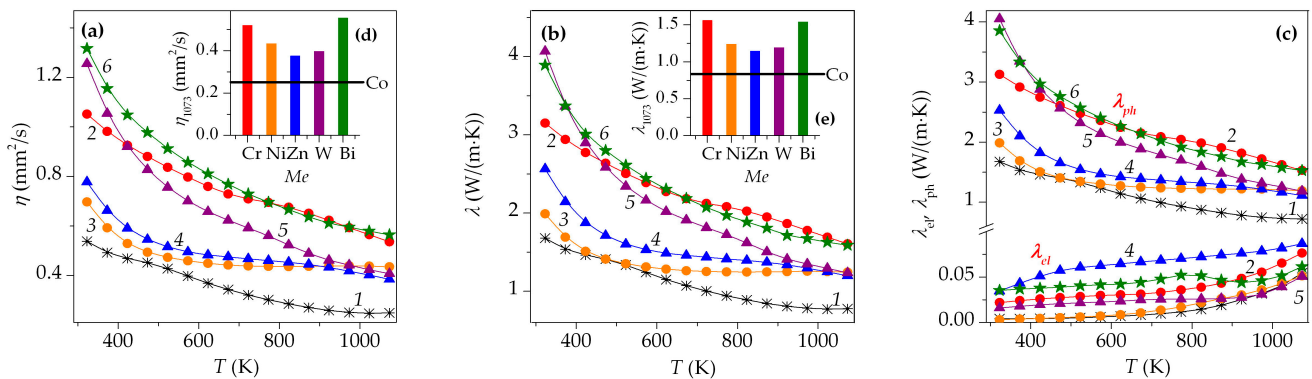


Figure 5. Temperature dependences of thermal diffusivity η (a), total thermal conductivity λ (b), lattice λ_{lat} and electron λ_{el} contributions, and (c) in thermal conductivity of ceramic samples of $\text{Na}_{0.55}\text{CoO}_2$ sodium cobaltite (1) and $\text{Na}_{0.55}\text{Co}_{0.90}\text{M}_{0.10}\text{O}_2$ ($M = \text{Cr}$ (2), Ni (3), Zn (4), W (5), and Bi (6)) solid solutions. Insets show the thermal diffusivity η_{1073} (d) and total thermal conductivity λ_{1073} (e) values of $\text{Na}_{0.55}\text{Co}_{0.90}\text{M}_{0.10}\text{O}_2$ solid solutions compared to the $\text{Na}_{0.55}\text{CoO}_2$ sodium cobaltite.

Figure of merit values of the studied ceramics sharply increased with the temperature increase and doping of layered sodium cobaltite by different transition and heavy metal oxides (Figure 6 and Table 2). The maximum thermoelectric performance was demonstrated for the $\text{Na}_{0.55}\text{Co}_{0.90}\text{W}_{0.10}\text{O}_2$ and $\text{Na}_{0.55}\text{Co}_{0.90}\text{Bi}_{0.10}\text{O}_2$ complex. Their ZT values reached 0.643 and 0.702 at 1073 K, which is 2.76 and 3.01 times larger than for the parent $\text{Na}_{0.55}\text{CoO}_2$ phase.

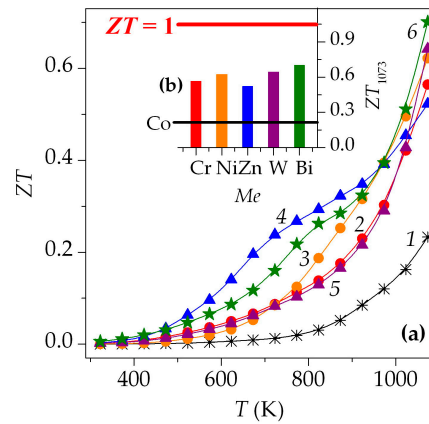


Figure 6. Temperature dependences of figure of merit ZT (a) of ceramic samples of $\text{Na}_{0.55}\text{CoO}_2$ sodium cobaltite (1) and $\text{Na}_{0.55}\text{Co}_{0.90}\text{M}_{0.10}\text{O}_2$ ($M = \text{Cr}$ (2), Ni (3), Zn (4), W (5), and Bi (6)) solid solutions. Insets show the figure of merit ZT_{1073} (b) values of $\text{Na}_{0.55}\text{Co}_{0.90}\text{M}_{0.10}\text{O}_2$ solid solutions compared to the unsubstituted $\text{Na}_{0.55}\text{CoO}_2$ phase.

Thus, the obtained results show the effectiveness of the doping strategy used in this work to enhance the thermoelectric characteristics of layered sodium cobaltite and give the possibility of recommending $\text{Na}_{0.55}\text{Co}_{0.90}M_{0.10}\text{O}_2$ ($M = \text{W}, \text{Bi}$) ceramics as the prospective material for *p*-branches of high-temperature thermoelectric devices used for the effective and direct conversion of heat into electrical energy.

4. Conclusions

Summarizing the results of the present contribution, partial substitution of Co by different transitions (Cr, Ni, and Zn) or heavy metals (W and Bi) in $\text{Na}_{0.55}\text{CoO}_2$ (up to 10 mol.%) retains the crystal structure of this phase unchanged and slightly affects its lattice constants, but increases the chemical stability, coherent scattering area, grain size, and grain orientation degree of $\text{Na}_{0.55}\text{Co}_{0.90}M_{0.10}\text{O}_2$ solid solutions compared to the unsubstituted $\text{Na}_{0.55}\text{CoO}_2$ phase. Such a substitution leads to the decrease of the values of electrical resistivity of $\text{Na}_{0.55}\text{Co}_{0.90}M_{0.10}\text{O}_2$ ceramics, and an increase in their thermal diffusivity, thermal conductivity, and the Seebeck coefficient values. The maximum *S* values possess $\text{Na}_{0.55}\text{Co}_{0.90}\text{W}_{0.10}\text{O}_2$ and $\text{Na}_{0.55}\text{Co}_{0.90}\text{Bi}_{0.10}\text{O}_2$ materials (620 and 666 $\mu\text{V/K}$ at 1073 K, respectively), which are 2.18 and 2.33 times larger, than for the base $\text{Na}_{0.55}\text{CoO}_2$ phase. As a result, the power factor and figure of merit values of $\text{Na}_{0.55}\text{Co}_{0.90}M_{0.10}\text{O}_2$ solid solutions are essentially higher than those for $\text{Na}_{0.55}\text{CoO}_2$ sodium cobaltite, and the maximum thermoelectric performance demonstrates $\text{Na}_{0.55}\text{Co}_{0.90}\text{W}_{0.10}\text{O}_2$ and $\text{Na}_{0.55}\text{Co}_{0.90}\text{Bi}_{0.10}\text{O}_2$ compounds, where *ZT* values at 1073 K reach 0.643 and 0.702, which is 2.76 and 3.01 times larger than those for the $\text{Na}_{0.55}\text{CoO}_2$ phase. The obtained results demonstrate the effectiveness of the doping strategy for the enhancement of the thermoelectric performance of layered sodium cobaltite derivatives. Materials possessing the best thermoelectric characteristic among the studied samples ($\text{Na}_{0.55}\text{Co}_{0.90}\text{W}_{0.10}\text{O}_2$ and $\text{Na}_{0.55}\text{Co}_{0.90}\text{Bi}_{0.10}\text{O}_2$) can be used as *p*-branches of high-temperature thermoelectric modules and generators, as well as *p*-legs of ceramic (oxide) thermocouples.

Supplementary Materials: The following supporting information can be downloaded at <https://www.mdpi.com/article/10.3390/solids5020017/s1>: Table S1: Chemical composition of ceramic samples of layered cobaltite of $\text{Na}_{0.55}\text{CoO}_2$ and $\text{Na}_{0.55}\text{Co}_{0.90}M_{0.10}\text{O}_2$ ($M = \text{Cr}, \text{Ni}, \text{Zn}, \text{and W}$) solid solutions.

Author Contributions: Conceptualization, A.I.K.; methodology, A.I.K., E.A.C. and N.S.K.; software, N.S.K.; validation, A.I.K. and E.A.C.; formal analysis, N.S.K. and E.A.C.; investigation, N.S.K., L.E.E., N.N.G. and A.V.P.; resources, A.I.K.; data curation, A.I.K.; writing—original draft preparation, N.S.K. and A.I.K.; writing—review and editing, A.I.K.; visualization, N.S.K.; supervision, A.I.K.; project administration, A.I.K.; funding acquisition, A.I.K. and N.S.K. All authors have read and agreed to the published version of the manuscript.

Funding: This work was supported by the Ministry of Education of the Republic of Belarus under project number 20111575 and by the Belarusian Republican Foundation for Fundamental Research, under project number 20122443.

Data Availability Statement: All data generated or analyzed during this study are included in this published article.

Acknowledgments: The authors would like to thank Dzmitry S. Kharytonau for fruitful discussions of research results and Dzmitry S. Darashchuk for technical support.

Conflicts of Interest: The authors declare no conflicts of interest.

References

- Prado-Gonjal, J.; López, C.A.; Pinacca, R.M.; Serrano-Sánchez, F.; Nemes, N.M.; Dura, O.J.; Martínez, J.L.; Fernández-Díaz, M.T.; Alonso, J.A. Correlation between crystal structure and thermoelectric properties of $\text{Sr}_{1-x}\text{Ti}_{0.9}\text{Nb}_{0.1}\text{O}_{3-\delta}$ ceramics. *Crystals* **2020**, *10*, 100. [[CrossRef](#)]
- Flitcroft, J.M.; Pallikara, I.; Skelton, J. Thermoelectric Properties of Pnma and Rocksalt SnS and SnSe. *Solids* **2022**, *3*, 155–176. [[CrossRef](#)]
- Yu, J.; Chen, K.; Azough, F.; Alvarez-Ruiz, D.T.; Reece, M.I.; Freer, R. Enhancing the thermoelectric performance of calcium cobaltite ceramics by tuning composition and processing. *ACS Appl. Mater. Interfaces* **2020**, *12*, 47634–47646. [[CrossRef](#)] [[PubMed](#)]

4. Zhang, W.; Zhu, K.; Liu, J.; Wang, J.; Yan, K.; Liu, P.; Wang, Y. Influence of the phase transformation in Na_xCoO_2 ceramics on thermoelectric properties. *Ceram. Int.* **2018**, *44*, 17251–17257. [[CrossRef](#)]
5. Li, Z.; Xiao, C.; Xie, Y. Layered thermoelectric materials: Structure, bonding, and performance mechanisms. *Appl. Phys. Rev.* **2020**, *9*, 011303. [[CrossRef](#)]
6. Chen, W.-H.; Lin, Y.-K.; Luo, D.; Jin, L.; Hoang, A.T.; Saw, L.H.; Nižetič, S. Effects of material doping on the performance of thermoelectric generator with/without equal segments. *Appl. Energy* **2023**, *350*, 121709. [[CrossRef](#)]
7. Koumoto, K.; Terasaki, I.; Funahashi, R. Complex oxide materials for potential thermoelectric applications. *MRS Bull.* **2006**, *31*, 206–210. [[CrossRef](#)]
8. Han, Y.; Ruan, Y.; Xue, M.; Wu, Y.; Shi, M.; Song, Z.; Zhou, Y.; Teng, J. Effect of annealing time on the cyclic characteristics of ceramic oxide thin film thermocouples. *Micromachines* **2022**, *13*, 1970. [[CrossRef](#)]
9. Ozkurt, B.; Madre, M.A.; Sotelo, A.; Portero, M.A.T. Enhanced thermoelectric properties in $\text{Bi}_2\text{Sr}_{2-x}\text{Ba}_x\text{Co}_2\text{O}_y$ by Ba doping. *Phys. B Condens. Matter* **2022**, *643*, 414138. [[CrossRef](#)]
10. Klyndyuk, A.; Chizhova, E.; Latypov, R.; Shevchenko, S.; Kononovich, V.M. Effect of the addition of copper particles on the thermoelectric properties of the $\text{Ca}_3\text{Co}_4\text{O}_{9+\delta}$ ceramics produced by two-step sintering. *Russ. J. Inorg. Chem.* **2022**, *67*, 237–244. [[CrossRef](#)]
11. Xiao, X.; Arif, S.; Ding, J.; Widenmeyer, M.; Constantinescu, G.; Kovalevsky, A.; Zhang, H.; Xie, W.; Weidenkaff, A. Molten salt synthesized La-substituted CaTiO_3 thermoelectric ceramics. *Open Ceram.* **2023**, *17*, 100522. [[CrossRef](#)]
12. Rubesova, K.; Jakes, V.; Jankovský, O.; Lojka, M.; Sedmidubský, D. Bismuth calcium cobaltite thermoelectrics: A study of precursor reactivity and its influence on the phase formation. *J. Phys. Chem. Solids* **2022**, *164*, 110631. [[CrossRef](#)]
13. Sotelo, A.; Rasekh, S.; Torres, M.A.; Bosque, P.; Madre, M.A.; Diez, J.C. Effect of synthesis methods on the $\text{Ca}_3\text{Co}_4\text{O}_9$ thermoelectric ceramic performances. *J. Solid State Chem.* **2015**, *221*, 247–254. [[CrossRef](#)]
14. Terasaki, I.; Sasago, Y.; Uchinokura, K. Large thermoelectric power in NaCo_2O_4 single crystals. *Phys. Rev. B* **1997**, *56*, R12685–R12687. [[CrossRef](#)]
15. Bresch, S.; Stargardt, P.; Moos, R.; Mieller, B. Co-fired multilayer thermoelectric generators based on textured calcium cobaltite. *Adv. Electron. Mater.* **2023**, *10*, 2300366. [[CrossRef](#)]
16. Molenda, J.; Baster, D.; Milewska, A.; Świerczek, K.; Bora, D.K.; Braun, A.; Tobola, J. Electronic origin of difference in discharge curve between Li_xCoO_2 and Na_xCoO_2 cathodes. *Solid State Ion.* **2014**, *271*, 15–27. [[CrossRef](#)]
17. Pohle, B.; Gorbunov, M.; Lu, Q.; Bahrami, A.; Nielsch, K.; Mikhailova, D. Structural and electrochemical properties of layered $\text{P}2\text{-Na}_{0.8}\text{Co}_{0.8}\text{Ti}_{0.2}\text{O}_2$ cathode in sodium-ion batteries. *Energies* **2022**, *15*, 3371. [[CrossRef](#)]
18. Nguyen, L.M.; Nguyen, V.H.; Nguyen, D.M.N.; Le, M.K.; Tran, V.M.; Le, M.L.P. Evaluating electrochemical properties of layered $\text{Na}_x\text{Mn}_{0.5}\text{Co}_{0.5}\text{O}_2$ obtained at different calcined temperatures. *Chemengineering* **2023**, *7*, 33. [[CrossRef](#)]
19. Baster, D.; Zajac, W.; Kondracki, Ł.; Hartman, F.; Molenda, J. Improvement of electrochemical performance of $\text{Na}_{0.7}\text{Co}_{1-y}\text{Mn}_y\text{O}_2$ -cathode material for rechargeable sodium-ion batteries. *Solid State Ion.* **2016**, *288*, 213–218. [[CrossRef](#)]
20. Banobre-López, M.; Rivadulla, F.; Caudillo, R.; López-Quintela, M.A.; Rivas, J.; Goodenough, J.B. Role of doping and Dimensionality in the Superconductivity of Na_xCoO_2 . *Chem. Mater.* **2005**, *17*, 1965–1968. [[CrossRef](#)]
21. Krasutskaya, N.S.; Klyndyuk, A.I.; Evseeva, L.E.; Tanaeva, S.A. Synthesis and properties of Na_xCoO_2 ($x = 0.55, 0.89$) oxide thermoelectrics. *Inorg. Mater.* **2016**, *52*, 393–399. [[CrossRef](#)]
22. Akram, R.; Khan, J.; Rafique, S.; Hussain, M.; Maqsood, A.; Naz, A.A. Enhanced thermoelectric properties of single phase Na doped Na_xCoO_2 thermoelectric material. *Mater. Lett.* **2021**, *300*, 130180. [[CrossRef](#)]
23. Rowe, D.M. *Thermoelectric Handbook Macro to Nano*; CRC Press Taylor and Francis Group: BocaRaton, FL, USA, 2006; 481p.
24. Kurniawan, I.; Prijamboedi, B. Enthalpy of formation of Na_xCoO_2 and $(\text{Na},\text{Mg})_x\text{CoO}_2$ systems: A first principle calculation study. *J. Phys. Conf. Ser.* **2019**, *1204*, 012028. [[CrossRef](#)]
25. Yang, X.; Wang, X.; Liu, J.; Hu, Z. Power factor enhancement in Na_xCoO_2 doped by Bi. *J. Alloys Compd.* **2014**, *582*, 59–63. [[CrossRef](#)]
26. Park, K.; Choi, J.W.; Lee, G.W.; Kim, S.-J.; Lim, Y.-S.; Choi, S.-M.; Seo, W.-S.; Lim, S.M. Thermoelectric properties of solution-combustion-processed $\text{Na}(\text{Co}_{1-x}\text{Ni}_x)_2\text{O}_4$. *Met. Mater. Int.* **2012**, *18*, 1061–1065. [[CrossRef](#)]
27. Pršić, S.; Savić, S.M.; Branković, Z.; Vrtnik, S.; Dapčević, A.; Branković, Z. Mechanochemically assisted solid-state and citric acid complex syntheses of Cu-doped sodium cobaltite ceramics. *J. Alloys Compd.* **2015**, *640*, 480–487. [[CrossRef](#)]
28. Zhou, R.; Li, J.; Wei, W.; Li, X.; Luo, M. Atomic substituents effect on boosting desalination performances of Zn-doped Na_xCoO_2 . *Desalination* **2020**, *496*, 114695. [[CrossRef](#)]
29. Nojiri, Y.; Ohtaki, M. Site-selective substitution by transition metal cations for NaCo_2O_4 via ion-exchange. *J. Ceram. Soc. Jpn.* **2005**, *113*, 400–404. [[CrossRef](#)]
30. Ito, M.; Furumoto, D. Microstructure and thermoelectric properties of $\text{Na}_x\text{Co}_2\text{O}_4/\text{Ag}$ composite synthesized by the polymerized complex method. *J. Alloys Compd.* **2008**, *450*, 517–520. [[CrossRef](#)]
31. Seetawan, T.; Amornkitbamrung, V.; Burinprakhon, T.; Maensiri, S.; Kurosaki, K.; Muta, H.; Uno, M.; Yamanaka, S. Thermoelectric power and electrical resistivity of Ag-doped $\text{Na}_{1.5}\text{Co}_2\text{O}_4$. *J. Alloys Compd.* **2006**, *407*, 314–317. [[CrossRef](#)]
32. Nakhowong, R. Effect of reduced graphene oxide on the enhancement of thermoelectric power factor of $\gamma\text{-Na}_x\text{Co}_2\text{O}_4$. *Mater. Sci. Eng. B* **2020**, *261*, 114679. [[CrossRef](#)]

33. Tsuruta, A.; Tanaka, M.; Mikami, M.; Kinemuchi, Y.; Masuda, Y.; Shin, W.; Terasaki, I. Development of $\text{Na}_{0.5}\text{CoO}_2$ thick film prepared by screen-printing process. *Materials* **2020**, *13*, 2805. [[CrossRef](#)] [[PubMed](#)]
34. Matsubara, I.; Zhou, Y.; Takeuchi, T.; Funahashi, R.; Shikano, M.; Murayama, N.; Shin, W.; Izu, N. Thermoelectric properties of spark-plasma-sintered $\text{Na}_{1+x}\text{Co}_2\text{O}_4$ ceramics. *J. Ceram. Soc. Jpn.* **2003**, *111*, 238–241. [[CrossRef](#)]
35. Chen, C.; Zhang, T.; Donelson, R.; Chu, D.; Tan, T.T.; Li, S. Thermoelectric properties of $\text{Na}_{0.8}\text{Co}_{1-x}\text{Fe}_x\text{O}_2$ ceramic prepared by spark plasma sintering. *Ceram. Mater. Energy Appl.* **2015**, *35*, 35–41. [[CrossRef](#)]
36. Klyndyuk, A.I.; Krasutskaya, N.S.; Chizhova, E.A.; Evseeva, L.E.; Tanaeva, S.A. Synthesis and properties of $\text{Na}_{0.55}\text{Co}_{0.9}M_{0.1}\text{O}_2$ ($M = \text{Sc}, \text{Ti}, \text{Cr-Zn}, \text{Mo}, \text{W}, \text{Pb}, \text{Bi}$) solid solutions. *Glass Phys. Chem.* **2016**, *42*, 100–107. [[CrossRef](#)]
37. Krasutskaya, N.; Klyndyuk, A. Effect of cobalt substitution on the microstructure and properties of $\text{Na}_{0.9}\text{CoO}_2$. *J. Thermoelectr.* **2012**, *4*, 39–44.
38. Klyndyuk, A.I.; Krasutskaya, N.S.; Dyatlova, E.M. Influence of sintering temperature on the properties of Na_xCoO_2 ceramics. *Proc. BSTU.* **2010**, *XVIII*, 99–102. (In Russian)
39. Viciu, L.; Huang, Q.; Cava, R.J. Stoichiometric oxygen content in Na_xCoO_2 . *Phys. Rev. B* **2006**, *73*, 212107. [[CrossRef](#)]
40. Joo, W.; Yoo, H.-I. Point defect structure of $\gamma\text{-Na}_x\text{CoO}_2$. *Solid State Ion.* **2018**, *314*, 74–80. [[CrossRef](#)]
41. Paytnitsky, I.V. *Analytical Chemistry of Cobalt*; Science: Moscow, Russia, 1965; 292p. (In Russian)
42. Seema, Kumar, N.; Chand, S. Structural, morphological, optical and dielectric properties of $\text{Ti}_{1-x}\text{Fe}_x\text{O}_2$ nanoparticles synthesized using sol-gel method. *J. Sol-Gel Sci. Technol.* **2022**, *105*, 163–175. [[CrossRef](#)]
43. Jalil, M.T.; Harbbi, K.H. Using the size strain plot method to specify lattice parameters. *Haitham J. Pure Appl. Sci.* **2023**, *36*, 123–129. [[CrossRef](#)]
44. Lotgering, F.K. Topotactical Reactions with Ferrimagnetic Oxides Having Hexagonal Crystal structures I. *J. Inorg. Nucl. Chem.* **1959**, *9*, 113–123. [[CrossRef](#)]
45. Zorkovská, A.; Feher, A.; Sébek, J.; Šantavá, E.; Bradaric, I. Non-Fermi-liquid behavior in the layered Na_xCoO_2 . *Low Temp. Phys.* **2007**, *33*, 944–947. [[CrossRef](#)]
46. Delmas, C.; Braconnier, J.-J.; Fouassier, C.; Hagenmuller, P. Electrochemical intercalation of sodium in Na_xCoO_2 bronzes. *Solid State Ion.* **1981**, *3–4*, 165–169. [[CrossRef](#)]
47. Zhou, R.; Guo, X.; Li, X.; Kang, Y.; Luo, M. An insight into the promotion effect of Na^+ /vacancy ordering on desalination performance of Na_xCoO_2 . *Desalination* **2020**, *478*, 114301. [[CrossRef](#)]
48. Tahashi, M.; Ogawa, K.; Takahashi, M.; Goto, H. Effect of compositional ratio of cobalt to calcium on crystal phase and thermoelectric properties of oxide thermoelectric material composed of sintered $\text{Ca}_3\text{Co}_4\text{O}_9/\text{Ca}_3\text{Co}_2\text{O}_6$ mixture. *J. Ceram. Soc. Jpn.* **2013**, *121*, 444–447. [[CrossRef](#)]
49. Lin, Y.-H.; Lan, J.; Shen, Z.; Liu Yu Nan, C.-W.; Li, J.-F. High-temperature electrical transport behaviors in textured $\text{Ca}_3\text{Co}_4\text{O}_9$ -based polycrystalline ceramics. *Appl. Phys. Lett.* **2009**, *94*, 072107. [[CrossRef](#)]
50. Klyndyuk, A.I.; Krasutskaya, N.S.; Chizhova, E.A. Synthesis and thermoelectric properties of ceramics based on $\text{Bi}_2\text{Ca}_2\text{Co}_{1.7}\text{O}_y$ oxide. *Glass Phys. Chem.* **2018**, *44*, 100–107. [[CrossRef](#)]
51. Koshibae, W.; Tsutsui, K.; Maekawa, S. Thermopower in cobalt oxides. *Phys. Rev. B* **2000**, *62*, 6869–6872. [[CrossRef](#)]
52. Klyndyuk, A.I.; Matsukevich, I.V. Synthesis, structure, and properties of $\text{Ca}_3\text{Co}_{3.85}M_{0.15}\text{O}_{9+\delta}$ ($M = \text{Ti-Zn}, \text{Mo}, \text{W}, \text{Pb}, \text{Bi}$) layered thermoelectrics. *Inorg. Mater.* **2015**, *51*, 944–950. [[CrossRef](#)]

Disclaimer/Publisher’s Note: The statements, opinions and data contained in all publications are solely those of the individual author(s) and contributor(s) and not of MDPI and/or the editor(s). MDPI and/or the editor(s) disclaim responsibility for any injury to people or property resulting from any ideas, methods, instructions or products referred to in the content.